Article:
Li, H. and Zhu, Z.Q. orcid.org/0000-0001-7175-3307 (2018) Influence of adjacent teeth magnet polarities on performance of flux reversal permanent magnet machine. IEEE Transactions on Industry Applications. ISSN 0093-9994

https://doi.org/10.1109/TIA.2018.2867818

Influence of Adjacent Teeth Magnet Polarities on Performance of Flux Reversal Permanent Magnet Machine

H. Y. Li, *Student Member, IEEE*, and Z. Q. Zhu, *Fellow, IEEE*

***Abstract*—This paper provides a comprehensive analysis of performance difference among various kinds of flux reversal permanent magnet (FRPM) machines having different PM arrangements. Four PM arrangement types are firstly identified by the number and relative polarities of PMs on the stator teeth, and their influence on equivalent pole-pair number of armature winding and working harmonics of air-gap field is revealed. Then, the torque variation against rotor pole number of each PM arrangement is analyzed. Detailed electromagnetic performance of four PM arrangements with 14-pole rotor is compared. It shows that the FRPM machine, in which four PM pieces are mounted on each stator tooth and two adjacent magnets on different stator teeth are of opposite polarities, offers the highest torque density and the highest efficiency, which makes it promising in low-speed high-torque applications. In addition, four prototype machines are manufactured and tested to validate the findings.**

***Index Terms*—flux reversal, magnet arrangement, torque proportion, winding factor**

I. Introduction

Stator-permanent magnet (PM) machines feature a salient pole rotor without coils or PMs and a possible high rotor pole number, which make them suitable for low-speed and high-torque applications where high torque density, high mechanical strength and good heat dissipation are required [1-3]. In comparison with other two kinds of stator-PM machines, i.e. doubly salient PM (DSPM) machine [4] and switched flux PM (SFPM) machine [5], a flux reversal PM (FRPM) machine is characterized by rigid stator structure, thus exhibiting promising prospect in various applications [6-8]. Fig. 1 shows the conventional three-phase FRPM machine, in which two PM pieces are mounted on the inner surface of each stator tooth and the concentrated-windings (CW) are normally adopted, resulting in short end windings.

In general, compared to SFPM machines, the torque density of FRPM machines is relatively low since the surface-mounted PM (SPM) structure increases the equivalent air-gap length, which will impair the rotor-tooth modulation effect [1]. To date, numerous efforts have been made to analyze and improve the performance of FRPM machines. Firstly, many feasible stator slot and rotor pole combinations have been identified [9, 10]. Secondly, the full-pitch distributed-windings (DW) with high winding factor can be adopted to improve the torque density in some slot/pole combinations [11-13]. Thirdly, several PM structures other than the SPM structure are proposed. Both inset PM structure [14] and consequent-pole PM structure [15] are beneficial to reduce the PM volume. In addition, the working principle of the FRPM machine is recently analyzed based on a magnetic gear [16], and its inherent relationship and similarities with other magnetically geared machines, e.g. SFPM machine, Vernier machine etc., are then revealed, from which the superiority of the FRPM machine for low-speed high-torque applications can be verified [3, 17-22].

Except for the foregoing research scopes, the PM arrangement of the FRPM machine is worthy of further investigation since it directly affects the air-gap field distribution and corresponding performance [23, 24]. The most conventional PM arrangement is shown in Fig. 2(a). A pair of PM pieces of alternate polarity is mounted on the inner surface of each stator tooth and the polarities of two adjacent magnets belonging to two stator teeth are identical. Thus, the PM arrangement is designated as NS-SN. Another PM arrangement (denoted as NS-NS) is shown in Fig. 2(b), in which two PM pieces are mounted on each stator tooth but the polarities of two adjacent magnets on different stator teeth are opposite. In addition, Figs. 2(c), (d) show other two PM arrangements by mounting two pairs of PM pieces on a single stator tooth. The two adjacent magnets on different stator teeth have identical polarities in NSNS-SNSN, but opposite polarities in NSNS-NSNS. Although NS-SN, NS-NS and NSNS-SNSN have been mentioned separately [7, 9, 25], the existing papers are all focused on the performance of a single machine with one specific PM arrangement instead of comparing the influence of different PM arrangements. Therefore, this paper aims to provide a comprehensive analysis of performance difference among FRPM machines having different PM arrangements. In addition, the NSNS-NSNS topology is proposed and found to be the most promising arrangement in terms of torque density and efficiency.

The authors are with the Department of Electronic and Electrical Engineering, The University of Sheffield, Sheffield S1 4DE, U.K. (e-mail: hli53@ sheffield.ac.uk; z.q.zhu@ sheffield.ac.uk).

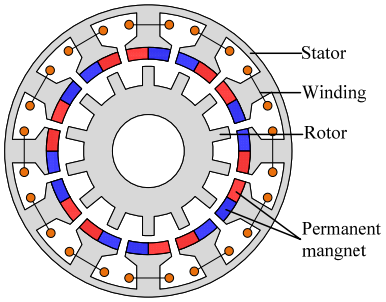

Fig. 1. Cross section of a conventional FRPM machine.

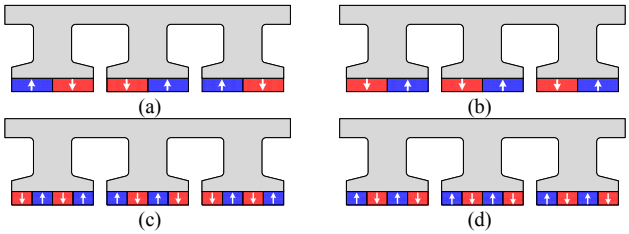

Fig. 2. Different PM arrangements. (a) NS-SN. (b) NS-NS. (c) NSNS-SNSN. (d) NSNS-NSNS.

II. Working Principle of FRPM Machines with Different PM Arrangements

It is well known that in a conventional rotor-PM machine, the torque is produced by the interaction between the fundamental fields originated from PM magneto-motive force (MMF) and armature MMF. However, the working principle becomes more complex in a FRPM machine since both PM MMF and armature MMF are subjected to the rotor-tooth modulation [12], resulting in abundant field harmonics in the air-gap. The pole-pair numbers and rotational speeds of these harmonics can be expressed as [26, 27]

$$p_{m,k} = |mp + kN_r| \tag{1}$$

$$\Omega_{m,k} = \frac{mp}{mp + kN_r}\Omega_a + \frac{kN_r}{mp + kN_r}\Omega_r \tag{2}$$

where p is the fundamental pole-pair number of the PM MMF or armature MMF, m is the corresponding order of Fourier series, N_r is the rotor pole number, k is the order of Fourier series of permeance ratio produced by salient rotor teeth, Ω_a is the rotational speed of the fundamental armature MMF or PM MMF, and Ω_r is the mechanical rotational speed of the rotor.

A. Air-Gap Field Produced by PM MMF

From (1), it is obvious that PM arrangement directly affects the PM field since the fundamental pole-pair number of PM MMF (p_m) varies with PM arrangement. Four 14-rotor-pole FRPM machines with different PM arrangements shown in Fig. 2 are firstly optimized aiming at the maximum torque by using genetic-algorithm-based global optimization in Maxwell finite element (FE) software, and their key design parameters are listed in TABLE I. It should be noted that the copper loss of all the machines are fixed at 20W. In addition, the stator slot number N_s of the NS-SN and the NS-NS is 12, while for the NSNS-SNSN and the NSNS-NSNS, N_s=6.

The PM field distributions of the four machines are shown in Figs. 3-6, respectively. Based on (1), the harmonic orders of the PM MMF and permeance (m_1, k_1) are labelled as well. As can be seen from Fig. 3, for the NS-SN, p_m=N_s/2=6 and harmonics which are odd times of p_m exist, e.g., the 6th and the 18th. It should be noted that both the 6th (m_1=1) and the 18th (m_1=3) harmonics are of considerable magnitude due to the specific distribution of the PM MMF [10]. In addition, it is found that the PM MMF is mainly subjected to the modulation of the fundamental permeance distribution, i.e., k_1=1, thus producing additional field harmonics, e.g., the 4th, the 8th, and the 20th. In comparison with the NS-SN, there is a large variation of the PM field in the NS-NS, as shown in Fig. 4. For the NS-NS, p_m=N_s=12 and the $p_m{}^{th}$ harmonic is of the largest magnitude. In addition, considerable 2nd and 26th harmonics appear due to the rotor-tooth modulation.

In terms of the other two PM arrangements with four PM pieces on each stator tooth, more abundant PM field harmonics exist, as shown in Figs. 5, 6. For the NSNS-SNSN, p_m=N_s/2=3 and harmonics which are odd times of p_m always have large magnitude, particularly the 9th and the 15th, i.e., m_1=3 and 5. Similarly, additional harmonics appear due to the rotor-tooth modulation, e.g., the 1st, the 5th, and the 11th. For the NSNS-NSNS, p_m=N_s=6 and both odd- and even-times harmonics of p_m exist, e.g., the 6th, the 12th and the 18th. It should be noted that the 12th (m_1=2) has much larger magnitude than others. Again, abundant modulated harmonics emerge, e.g., the 2nd, the 4th, and the 8th.

In general, the PM fields of four PM arrangements are totally different due to the changed PM MMF distribution. For each arrangement, p_m and corresponding major PM field harmonics are summarized in TABLE II. As can be seen, p_m is N_s for NS-NS and NSNS-NSNS since the PM arrangements are exactly the same for two adjacent stator teeth while it is N_s/2 for NS-SN and NSNS-SNSN due to the different PM arrangements on two adjacent stator teeth. In terms of the major harmonics of the PM MMF and air-gap flux density, they are related to not only the relative polarities of the PMs but also the number of PM pieces. From Fig. 3, the major harmonics of NS-SN are the N_s/2th and the 3N_s/2th, while it is the N_sth for NS-NS (see Fig. 4). As for NSNS-SNSN, two major harmonics exist, which are the 3N_s/2th and the 5N_s/2th (Fig.5). In addition, the 2N_sth is the major harmonic in NSNS-NSNS (see Fig. 6).

TABLE I
Machine Parameters (units: mm)

	FEA models						Prototypes			
	NS-SN	NS-NS	NS-NS (DW)	NSNS-SNSN	NSNS-SNSN (DW)	NSNS-NSNS	NS-SN	NS-NS	NSNS-SNSN	NSNS-NSNS
D	90									
l	25									
h_r, u_r	1.2T, 1.05									
y_c	1	1	3	1	3	1	1	1	1	1
t_{sy}	2.1	3.2	3.3	4.8	6.5	3.3	3.2		4.2	
w_{st}	4	3	4.1	6.8	7.8	7.4	3.2		8.4	
w_{so}	2.5	1.9	2	4.6	4.6	4.1	2.5		2.5	
k_{sr}	0.7	0.67	0.69	0.65	0.66	0.66	0.65		0.65	
h_m	2	2	2	2	2	2	2		2	
w_{rt}	3.9	3.2	3.5	3.6	3.4	3.4	3.6		3.6	
l_{end}	27.6	26.6	74.1	51.7	139.8	53.1	26.4		52.4	
T_{avg}	1.35	1.60	3.04	2.21	3.66	2.59	1.21	1.43	2.02	2.30

D is the stator outer diameter, l is the axial length, h_r and u_r are the remeance and relative permeability of the PM, y_c is the coil pitch, t_{sy} is the thickness of

stator yoke, w_{st} is the width of stator teeth, w_{so} is the width of stator slot opening, k_{sr} is the split ratio, h_m is the PM thickness, w_{rt} is the width of rotor teeth, l_{end} is the end-winding length, and T_{avg} is the average torque.

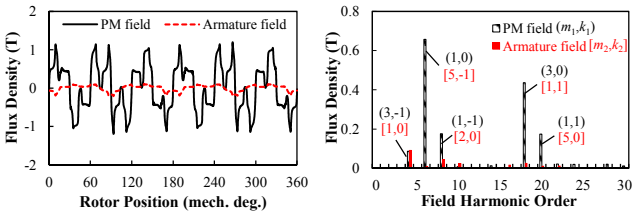

(a) (b)

Fig. 3. Air-gap flux density produced by the PM MMF and armature MMF in the NS-SN. (a) Waveforms. (b) Harmonic spectra.

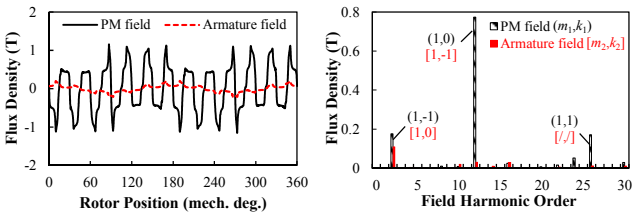

(a) (b)

Fig. 4. Air-gap flux density produced by the PM MMF and armature MMF in the NS-NS. (a) Waveforms. (b) Harmonic spectra.

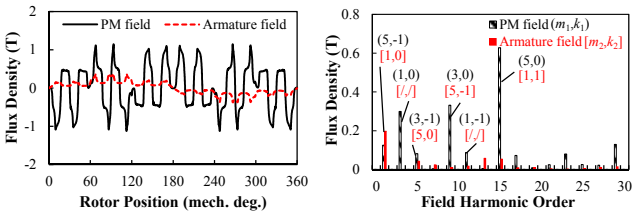

(a) (b)

Fig. 5. Air-gap flux density produced by PM MMF and armature MMF in the NSNS-SNSN. (a) Waveforms. (b) Harmonic spectra.

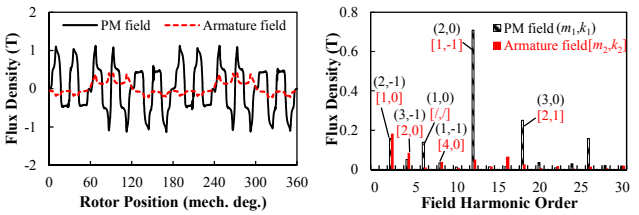

(a) (b)

Fig. 6. Air-gap flux density produced by PM MMF and armature MMF in the NSNS-NSNS. (a) Waveforms. (b) Harmonic spectra.

TABLE II
POLE-PAIR NUMBER OF FRPM MACHINES

PM arrangement	NS-SN	NS-NS	NSNS-SNSN	NSNS-NSNS
p_m	$N_s/2$	N_s	$N_s/2$	N_s
Major PM field	$N_s/2$, $3N_s/2$	N_s	$3N_s/2$, $5N_s/2$	$2N_s$
p_{eq}	$\min(\lvert N_s/2-N_r\rvert, \lvert 3N_s/2-N_r\rvert)$	$\lvert N_s-N_r\rvert$	$\min(\lvert 3N_s/2-N_r\rvert, \lvert 5N_s/2-N_r\rvert)$	$\lvert 2N_s-N_r\rvert$

B. *Equivalent Pole-Pair Number and Armature Field*

In [16], a FRPM machine of NS-SN arrangement is analyzed based on a 'fictitious' magnetic gear, from which the performance expressions are analytically derived. Further, the equivalent pole pair number p_{eq} of NS-SN is proposed in [10, 16], which reflects the flux distribution inside the stator and rotor core, and can be used to determine the winding connections according to the star of slots of the conventional rotor-PM machine, of which the fundamental pole-pair number of the armature winding is p_{eq}.

Since the PM arrangement directly determines the PM field, p_{eq} of four PM arrangements are totally different and significantly influence the winding connections and resulted armature field of the corresponding FRPM machine. Considering the fact that 1) the flux paths of air-gap PM field harmonics without rotor-tooth modulation mainly circle through the stator tooth-tips and the air-gap; 2) the air-gap PM field harmonics after rotor-tooth modulation and with relatively high pole-pair number are more likely to short-circuit through the stator tooth-tips and the rotor teeth, the fields circle through the stator yoke and rotor yoke are those subjected to the rotor-tooth modulation and with low pole pair number simultaneously. Based on the major PM field harmonics shown in Figs.3-6, p_{eq} of different PM arrangements can be obtained and summarized in TABLE II. Fig. 7 shows the no-load flux distributions and equivalent flux paths of the four FRPM machines. As can be seen, although all the machines have 14 rotor poles, the flux distributions in stator and rotor cores are totally different. For the NS-SN, p_{eq}=4; for the NS-SN, p_{eq}=2; for the NSNS-SNSN, p_{eq}=1; for the NSNS-NSNS, p_{eq}=2. The smaller p_{eq}, the longer magnetic length.

According to different p_{eq}, the winding connections of the four machines can be determined and the resulted armature fields are shown in Figs. 3-6. It should be noted that the concentrated windings are adopted in all the machines. Based on (1), the harmonic orders of the armature MMF and permeance [m_2, k_2] are also labelled. As can be seen, there are abundant harmonics of the armature field due to the armature MMF harmonics and the rotor-tooth modulation. By way of example, for the 12/14 stator-slot/rotor-pole NS-SN, p_{eq}=4, and the winding connection is equivalent to a conventional 12/8 stator-slot/rotor-pole rotor-PM machine. Therefore, both 1, 2, and 5-times harmonics of p_{eq} exist, i.e., the 4th, the 8th, and the 20th. After rotor-tooth modulation, additional field harmonics emerge, such as the 6th [m_2=5, k_2=-1] and the 18th [m_2=1, k_2=1]. Moreover, it is clearly shown that some armature field harmonics emerge in pairs with the PM field, which may contribute to the torque production.

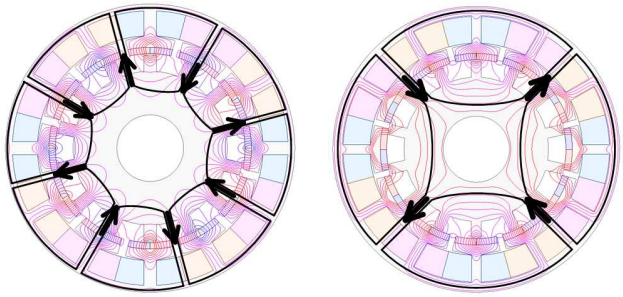

(a) (b)

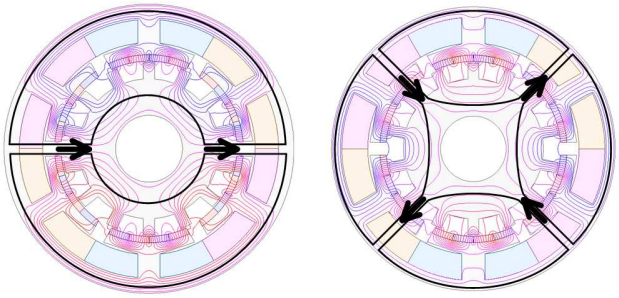

(c) (d)

Fig. 7. Field distributions and equivalent flux paths of the machines. (a) 12/14 NS-SN. (b) 12/14 NS-NS. (c) 6/14 NSNS-SNSN. (d) 6/14 NSNS-NSNS.

C. Torque Contribution of working Field Harmonics

For the machines working based on air-gap field modulation, although abundant field harmonics exist, only some of them contribute to the torque production. To identify the working harmonics in such machines, there are mainly two approaches. The first one is from the perspective of generator, i.e., only PM field is considered and the contribution to back-EMF of each harmonic can be analytically quantified. Based on this approach, the working harmonics of no-load air-gap PM field of NS-SN have been well analyzed in some papers [21, 24]. The second approach is from the perspective of motor, i.e., both PM field and armature field are considered, and the working field harmonics contributing to torque production can be directly obtained by using Maxwell stress tensor [28], as

$$T_n(t)=\frac{\pi R^2 L}{\mu_0}B_{rn}B_{tn}\cos\left[\theta_{rn}(t)-\theta_{tn}(t)\right] \quad (3)$$

where $T_n(t)$ is the instantaneous torque produced by the n^{th} harmonic, R is the air-gap radius, μ_0 is the vacuum permeability, L is the effective axial length, B_{rn} and B_{tn} are the magnitudes of the radial and tangential components of the n^{th} harmonic, $\theta_{rn}(t)$ and $\theta_{tn}(t)$ are the phases of the radial and tangential components of the n^{th} harmonic.

In this paper, the second approach is used to analyze and compare the working harmonics of different PM arrangements. Fig. 8 shows the torque contribution of each field harmonic in the four machines. It can be found that the torques of all the FRPM machines are contributed by several dominant working field harmonics regardless of PM arrangement, which is different from the conventional rotor-PM machine. However, the contribution of each harmonic and the machine average torque are largely related to the PM arrangement. It is well known that a steady torque component can be produced by the interaction of one PM field harmonic and one armature field harmonic when they have the same pole-pair number and rotational speed. The resulted torque is proportional to the product of the pole-pair number, magnitudes of both the PM and armature field harmonics, and the relative phase angle between them [29]. Based on Figs.3-6, 8, (1), and (2), the order, speed, torque proportion of dominant working harmonics (with torque contribution>3%), and the magnitudes of corresponding PM field and armature field harmonics are listed in TABLE III. As can be seen, for the NS-NS, the torque contribution is concentrated since mainly two working harmonics have considerable torque contribution. In contrast, for the other three PM arrangements, the torque contributions are more scattered with more than four dominating harmonics having proportion higher than 3%. It should be noted that although some harmonic pairs are static, i.e., the rotational speed is zero, a steady torque component can still be produced, which is similar with the SFPM machine analyzed in [28].

In terms of the total average torque of different PM arrangements, some findings can be concluded as:

1. The 12/14 NS-NS has higher torque than the 12/14 NS-SN. This can be explained by the fact that for the NS-NS, the magnitude of the 12th armature field is large which can interact with the absolutely dominant 12th PM field. In contrast, there are mainly two PM field harmonics with large magnitude in the NS-SN, i.e., the 6th and 18th. However, the 6th armature field is of very low magnitude, making the large 6th PM field not fully utilized.

2. The 6/14 NSNS-SNSN and NSNS-NSNS have higher torque than the other two PM arrangements with 12 stator slots. This phenomenon can be attributed to the large magnitude of armature field in the former two machines when concentrated-windings are adopted. By way of example, for both the 12/14 NS-NS and 6/14 NSNS-NSNS, p_{eq}= 2. However, the magnitude of the 2nd armature field is 0.11T in the former, which is much smaller than that in the latter (0.18T).

3. The 6/14 NSNS-NSNS has higher torque than the 6/14 NSNS-SNSN, thus exhibiting the highest average torque among four machines. The torque difference between two 6-slot-stator machines can be explained by the different torque contribution effects of the p_{eq}^{th} field harmonic. For the NSNS-NSNS, the 2nd field harmonic pair produces a positive torque component, thus boosting the torque while the 1st field harmonic pair of the NSNS-SNSN produces a negative torque component and impair the overall torque. This can be further explained by the rotational direction of the p_{eq}^{th} field harmonic. Based on (2), the 1st field harmonic of the NSNS-SNSN rotates to the reverse direction, producing a negative torque component, while the 2nd harmonic of the NSNS-NSNS is of positive rotation, thus producing a positive torque component.

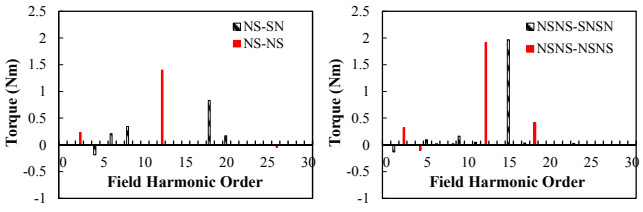

(a) (b)

Fig. 8. Torque contribution of field harmonics. (a) NS-SN and NS-NS. (b) NSNS-SNSN and NSNS-NSNS.

TABLE III
TORQUE PROPORTION OF WORKING HARMONICS

PM arrangement	$p_{m,k}$ & torque proportion	PM field & (m_1,k_1)	Armature field & $[m_2,k_2]$	Speed
NS-SN (T_{avg}=1.35Nm)	4th (-13.8%)	0.09T (3,-1)	0.09T [1,0]	-14/4Ω_r
	6th (15.6%)	0.66T (1,0)	0.01T [5,-1]	0
	8th (25.6%)	0.18T (1,-1)	0.04T [2,0]	14/8Ω_r
	18th (61.7%)	0.44T (3,0)	0.03T [1,1]	0
	20th (12.6%)	0.17T (1,1)	0.01T [5,0]	14/20Ω_r
NS-NS (T_{avg}=1.60Nm)	2nd (14.5%)	0.18T (1,-1)	0.11T [1,0]	14/2Ω_r
	12th (87.5%)	0.77T (1,0)	0.03T [1,-1]	0

NSNS-SNSN (T_{avg}=2.21Nm)	1st (-6.0%)	0.13T (5,-1)	0.20T [1,0]	-14/1Ω_r
	5th (4.4%)	0.08T (3,-1)	0.04T [5,0]	14/5Ω_r
	9th (7.4%)	0.33T (3,0)	0.01T [5,-1]	0
	15th (88.9%)	0.63T (5,0)	0.05T [1,1]	0
NSNS-NSNS (T_{avg}=2.59Nm)	2nd (12.4%)	0.16T (2,-1)	0.18T [1,0]	14/2Ω_r
	4th (-3.8%)	0.05T (3,-1)	0.08T [2,0]	14/4Ω_r
	12th (73.9%)	0.71T (2,0)	0.05T [1,-1]	0
	18th (16.0%)	0.25T (3,0)	0.02T [2,1]	0

III. Influence of Rotor Pole Number on Performance of FRPM Machines

The torque performance of a FRPM machine is significantly affected by the rotor pole number N_r. In [21], the influence of N_r on performance of NS-SN is investigated based on analytical equations. It is proven that the optimal N_r is 14 for 12-slot machines. In this paper, the influence of N_r on performance of FRPM machines regarding PM arrangement will be investigated based on finite element analysis (FEA).

A. Two Magnet Pieces on Each Stator Tooth

Fig. 9 shows the average torque variation against N_r of NS-SN and NS-NS. It should be noted that all the machines utilize concentrated-winding, and are optimized aiming at the maximum torque density under the fixed stator outer diameter, axial length and copper loss shown in TABLE I. As can be seen, both NS-SN and NS-NS have relatively high torque when N_r ranges from 8 to 20, and the torques are the highest when N_r=14. This can be explained by that 1) the back-EMF is proportional to N_r; 2) the flux of PMs can be sufficiently utilized when N_r is close to the number of PM pairs which is 12 in this case.

In addition, each PM arrangement shows its superiority in a specific range of N_r. When N_r ranges from 8 to 12, the torque of the NS-SN is higher while that of the NS-NS is higher within the range from 13 to 20. The winding factors of two machines are utilized to simply explain the different torque variation trends against N_r. Typically, two approaches can be adopted to calculate the winding factor. The first approach is that the FRPM machine can be regarded as the conventional rotor-PM machine with pole-pair number of p_{eq}, which is listed in TABLE II. Then the winding factor can be obtained, e.g. the winding factor of the 12/14 NS-SN is exactly the same as the conventional 12-stator-slot rotor-PM machine with pole pair number of PMs being 4, which is 0.866. Another approach is that the winding factor of the FRPM machine can be directly calculated by using the star of slots with additional consideration of relative polarities of adjacent stator teeth, which is similar to the winding factor calculation in SFPM machine [30]. In this paper, the winding factor of the FRPM machines will be calculated based on the second approach.

Fig. 10 shows the back-EMF phasors of the 12/14 NS-SN. Considering the opposite PM arrangement of two adjacent stator teeth and the influence on the phase shift of the back-EMF phasor, the phasors of the even-number slots are marked with a (‘), as shown in Fig. 10 (a). Correspondingly, the coil-EMF phasors of the double-layer concentrated-winding are shown in Fig. 10 (b). For the 12/14 NS-NS, since the PM arrangements of all stator teeth are identical, its star of slots is just the same as the conventional rotor-PM machine, as shown in Fig. 11 (a). Also, the coil-EMF phasors of the double-layer concentrated-winding are shown in Fig. 11 (b).

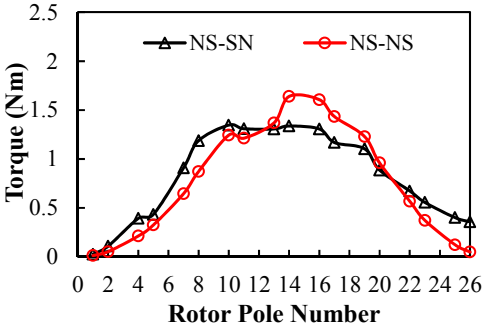

Fig. 9. Torque variation against N_r in NS-SN and NS-NS. (N_s=12)

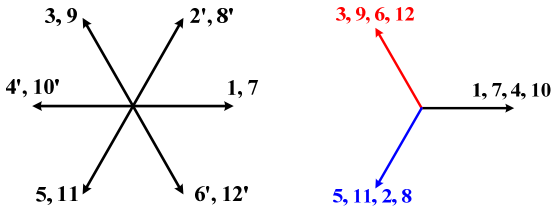

(a) (b)

Fig. 10. Back-EMF phasors of 12/14 NS-SN. (a) Star of slot. (b) Coil-EMF phasors.

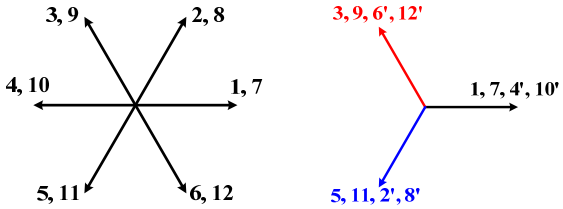

(a) (b)

Fig. 11. Back-EMF phasors of 12/14 NS-NS. (a) Star of slot. (b) Coil-EMF phasors.

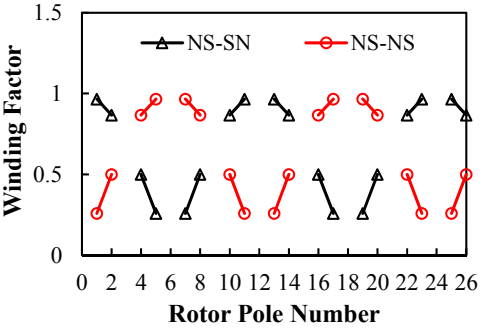

Fig. 12. Winding factors of NS-SN and NS-NS with different N_r.

Therefore, the distribution factor k_d of NS-SN and NS-NS are exactly the same, which is

$$k_d = \frac{\sin(Q\nu\alpha/2)}{Q\sin(\nu\alpha/2)} \tag{4}$$

where Q is the number of coil-EMF phasors per phase, α is the angle between two adjacent coil-EMF phasors, and ν is the harmonic order. For 12/14 FRPM machines with double-layer windings, Q=4 and α =0°. Hence, k_d=1 for the fundamental harmonic.

Considering the pitch factor of the concentrated winding, for NS-SN, the angular difference between two adjacent slot conductors for the v^{th} back-EMF harmonic is

$$\theta_c = v2\pi \, {N_r}/{N_s} \tag{5}$$

and for NS-NS, it is

$$\theta_c = v(2\pi \, {N_r}/{N_s} - \pi) \tag{6}$$

Hence, the pitch factor can be obtained as

$$k_q = \left|\cos(\theta_c / 2)\right| \tag{7}$$

Based on (4)-(7), the winding factors of NS-SN and NS-NS are shown in Fig. 12. Comparing Fig. 12 with Fig. 9, it is found that the different torque variation trends of NS-SN and NS-NS are largely related to the winding factors. When $15<N_r<20$, NS-NS has larger winding factor, resulting in higher torque; when $9<N_r<13$, NS-SN has larger winding factor and higher torque. When N_r=13 and 14, although the NS-SN has larger winding factor, its output torque is smaller than the NS-NS, which can be explained by the different working harmonics of two arrangements shown in Section II.

B. Four Magnet Pieces on Each Stator Tooth

Considering NSNS-SNSN and NSNS-NSNS, the torque variations against N_r are shown in Fig. 13. Both PM arrangements have relatively high torque when N_r ranges from 10 to 20, and the 13-pole-rotor is preferred for NSNS-SNSN while the 14-pole-rotor is the best for NSNS-NSNS in terms of torque. Again, this phenomenon can be explained by the winding factors shown in Fig. 14. For NSNS-SNSN, the winding factor is higher when N_r=13. For NSNS-NSNS, the winding factor is higher when N_r=14.

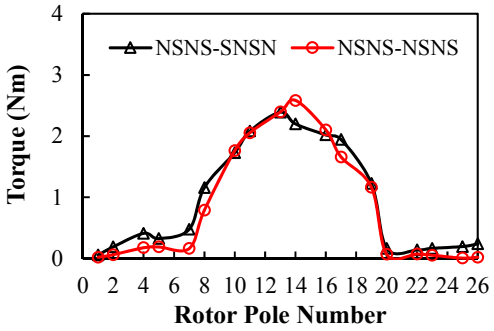

Fig. 13. Torque variation against N_r in NSNS-SNSN and NSNS-NSNS. (N_s=6)

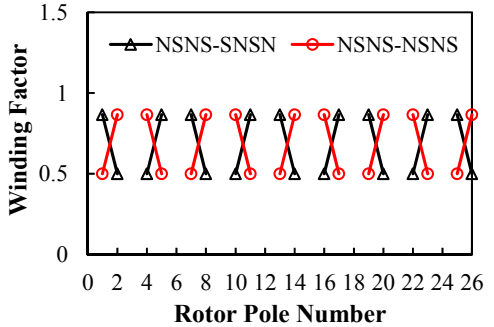

Fig. 14. Winding factors of NSNS-SNSN and NSNS-NSNS with different N_r.

IV. Performance Comparison of Four FRPM Machines

In the previous analysis, the optimal rotor pole number N_r of each PM arrangement has been identified, which is 13 for the 6-stator-slot NSNS-SNSN, and 14 for the 12-stator-slot NS-SN, 12-stator-slot NS-NS and 6-stator-slot NSNS-NSNS. It should be noted that the above conclusions are valid only when the concentrated-windings (CWs) are used. For some machines, the winding factor and average torque may be improved when integer-slot distributed-windings (DWs) are used [11] [12]. For instance, as shown in Figs. 12, 14, the winding factor of the 12/14 NS-NS and the 6/14 NSNS-SNSN is 0.5, and it can be improved to 1 when the short-pitch CWs are replaced with full-pitch DWs. Hence, additional two machines with DWs are optimized, and their parameters and performance are listed in TABLE I. As can be seen, the average torque T_{avg} of the 12/14 NS-NS with DWs is 90% higher than its CWs counterpart, and T_{avg} of the 6/14 NSNS-SNSN with DWs is also 66% higher than its CWs counterpart. However, it should be noted that all the machines are optimized under the same active copper loss (20W), i.e., only active part of the copper is considered while the end-winding length (l_{end}) is neglected. To achieve a more fair comparison, l_{end} of different machines are then calculated as

$$l_{end} = k_s \tau_y \tag{8}$$

where k_s is the empirical coefficient of the end-winding, which is selected as 1.25 for the two machines with DWs, and 1.35 for the other machines with CWs [31]; τ_y is the coil pitch of each machine, it is $\pi y_c(R_{co}+R_{ci})/12$ for the 12-stator-slot NS-NS and NS-SN, and $\pi y_c(R_{co}+R_{ci})/6$ for the 6-stator-slot NSNS-SNSN and NSNS-NSNS; y_c is the coil pitch, which is 1 for the machines with CWs and 3 for the two machines with DWs; R_{co}, R_{ci} are the outer radius and inner radius of the stator slot, respectively.

From TABLE I, it is clear that the machines with DWs have much larger l_{end} than those with CWs, especially for the 12/14 NSNS-SNSN. By considering l_{end}, the torques per copper loss of various machines under different active axial stack lengths (l) are compared in Fig. 15. As can be seen, for machines with DWs, the torque benefits brought by high winding factor are impaired and even cancelled due to long l_{end}, particularly when l is small [32]. For instance, when l<45mm, the NSNS-SNSN with CWs always has higher torque per copper loss than its counterpart with DWs; when l<30mm, torque per copper loss of the NS-NS with CWs is better.

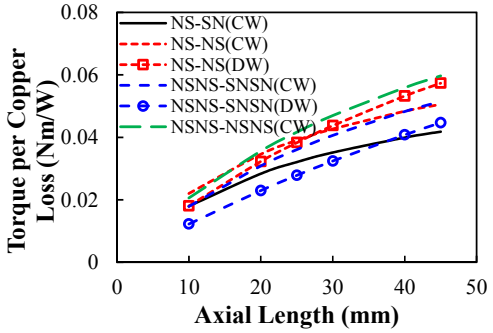

Fig. 15. Torque per copper loss under different active axial stack length l.

In addition, considering the fact that the machines with CWs have higher slot filling factor and are easier to manufacture, and the aim of this paper is to reveal the influence of PM arrangement on working harmonics and performance of the FRPM machine, only CWs are considered for all the PM arrangements. Detailed performance difference among four arrangements with associated optimal N_r will be investigated. Considering the fact that the torque of the 6-slot NSNS-SNSN with N_r=14 is close to the highest value when N_r=13, N_r is chosen as 14 for all the machines for simplicity.

The optimal parameters of the four machines are shown in TABLE I, and their cross-sections are shown in Fig. 16. As can be seen, the stator teeth of the NSNS-SNSN and NSNS-NSNS are wider than those of the NS-SN and NS-NS since the flux through one stator tooth is much more due to the increased number of PM pieces mounted on single stator tooth. In addition, there has a big difference of the ratio between the stator yoke thickness and the stator tooth width. For the NS-SN, the ratio is around 0.5 while that is larger than 1 for the NS-NS. This can be explained by p_{eq}, since for 12/14 NS-NS, p_{eq}=2 and for 12/14 NS-SN, p_{eq}=4. The smaller p_{eq}, the longer magnetic path, and the thicker stator yoke. Similarly, the stator yoke of the NSNS-NSNS is thinner than the NSNS-SNSN, thanks to the larger p_{eq}. Besides, it should be noted that the obtained optimal magnet thicknesses for all the machines are smaller than 2mm so as to reduce the equivalent air-gap length. However, the magnet thickness is chosen as 2mm due to the consideration of manufacturing feasibility and anti-demagnetization capability.

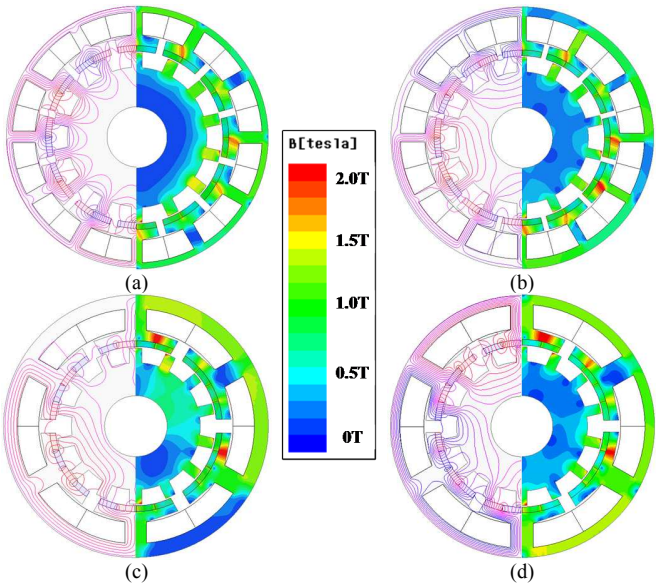

Fig. 16. Cross-sections, and full-load field distributions. (a) NS-SN. (b) NS-NS. (c) NSNS-SNSN. (d) NSNS-NSNS.

A. No-Load Performance

When the rotor speed is 1000rpm and the winding turns per phase N_{ph} are 4, the no-load back-EMFs are shown in Fig. 17. As can be seen, the back-EMFs of machines with four magnet pieces on each stator tooth are much larger than the other two machines with two magnet pieces on each stator tooth. For instance, the proposed NSNS-NSNS has the highest back-EMF, which is 98% higher than the conventional NS-SN. In addition, the 2nd and 3rd harmonics exist in the NSNS-SNSN and NSNS-NSNS due to the harmonics of the permeance ratio, which may cause larger torque pulsation.

Fig. 18 shows the cogging torque of the four machines. Clearly, different PM arrangements have a big influence on the cogging torque. As can be seen, the fundamental orders of the cogging torque of the NS-SN and NS-NS are 6 while those of the NSNS-SNSN and NSNS-NSNS are 3. In addition, the NS-NS has the lowest cogging torque while the NSNS-SNSN and NSNS-NSNS have the largest. Therefore, for the applications where low torque ripple is required, the cogging torque reduction techniques should be utilized especially for the NSNS-SNSN and NSNS-NSNS [33].

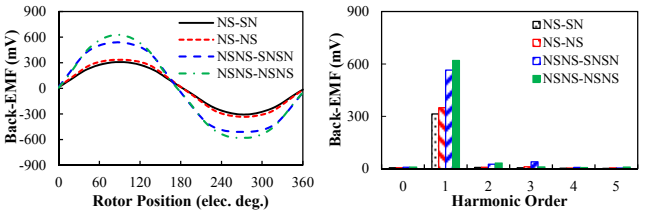

Fig. 17. Phase back-EMF of four FRPM machines (n=1000rpm, N_{ph}=4). (a) Waveforms. (b) Harmonic spectra.

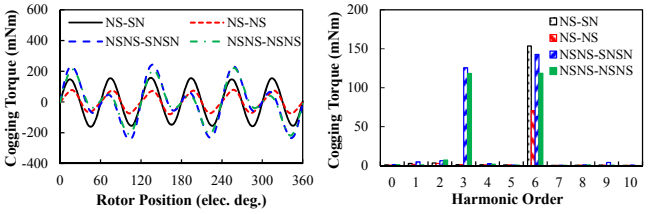

Fig. 18. Cogging torque of four FRPM machines. (a) Waveforms. (b) Harmonic Spectra.

B. Torque Performance

When copper loss p_{cu}=20W, the rated torques of the machines are shown in Fig. 19. The average torque of the proposed NSNS-NSNS is 2.6Nm, which is the highest and 93% higher than the lowest one of NS-SN arrangement. In addition, it should be noted that the torque ripples of the NSNS-SNSN and NSNS-NSNS are relatively larger especially compared to the NS-NS, which is resulted from the larger cogging torque and additional 2nd harmonic of the back-EMF. However, this problem can be effectively eliminated by various methods aiming at torque ripple minimization [33]. The full-load field distributions and flux densities of four machines are also shown in Fig. 16. It shows that the flux paths in the stator and rotor significantly vary with PM arrangement, which can be characterized by p_{eq}. In addition, for all the machines, the flux density in rotor teeth and stator tooth tips is higher than other regions.

By setting the rated torque of each machine as benchmark, the over-load capability of the machines is shown in Fig. 20. As can be seen, the over-load capability of the NSNS-NSNS and NSNS-SNSN is inferior to the NS-SN and NS-NS while that of the NS-NS is the best. This can be explained by the different self-inductances of the machines (see Fig. 21). It should be

noted that the winding turns per phase N_{ph} are same for all the machines, which are 4. As can be seen, the self-inductances of all the machines decrease with current due to the saturation, and the self-inductances of the NSNS-SNSN and the NSNS-NSNS are similar, which are much higher than those of the NS-SN and the NS-NS. In addition, the NS-NS has the smallest self-inductance. The larger the self-inductance, the higher the armature field, the severer the saturation, and the worse the over-load capability.

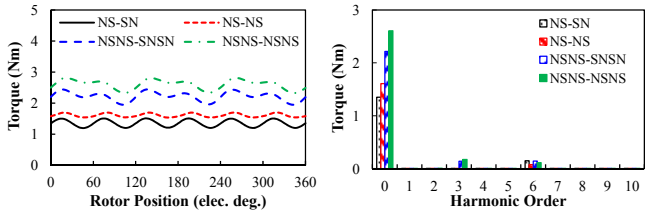

Fig. 19. Rated torque of four FRPM machines (p_{cu}=20W). (a) Waveforms. (b) Harmonic spectra.

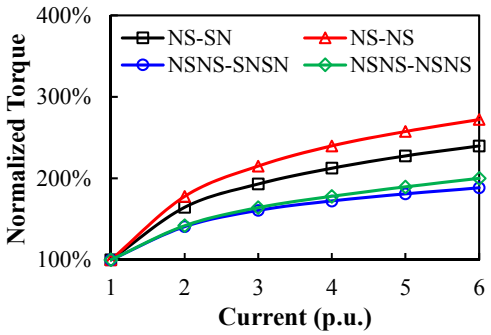

Fig. 20. Torque variation against current.

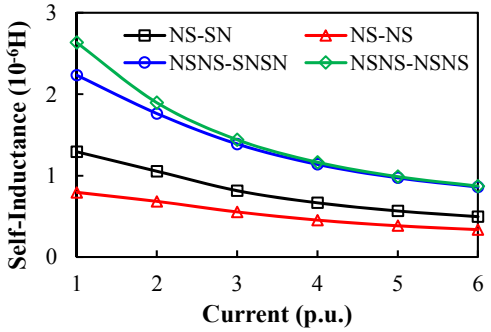

Fig. 21. Inductance variation against current. (N_{ph}=4)

C. Losses and Efficiency

Fig. 22 shows the full-load iron loss variation against speed. As can be seen, the loss rapidly increases with speed, and it is higher in the NSNS-SNSN and NSNS-NSNS due to higher average flux density in the stator (see Fig. 16) when compared to the NS-SN and NS-NS. At n=3000rpm, detailed iron loss distribution is shown in Fig. 23. It shows that the stator yoke together with the stator teeth account for the most proportion of the iron loss regardless of the PM arrangement and load condition. In terms of the losses of different PM arrangements, they are largely related to p_{eq}. Under no-load condition, the flux density in the stator and iron loss are determined by the PM field only. For the NS-NS, p_{eq}=2 and it is smaller than that of the NS-SN which is 4. Therefore, the iron loss of the NS-NS is larger due to the longer magnetic path and corresponding higher average flux density in the stator yoke. When the machine operates under full-load condition, the flux density in the stator and iron loss are largely influenced by the armature field. For the NS-NS, the winding connection is equivalent to a conventional 12/4 rotor-PM machine while it is equivalent to a 12/8 PM machine for the NS-SN. It is well known that the harmonics of the armature field of a 12/4 PM machine are smaller than a 12/8 PM machine [32]. Therefore, the iron loss produced by the armature field is smaller in the NS-NS. Similarly, the winding connection of the NSNS-SNSN is equivalent to a 6/2 PM machine while it is equivalent to a 6/4 PM machine for the NSNS-NSNS. Therefore, the iron loss produced by the armature field of the NSNS-NSNS is larger than that of the NSNS-SNSN due to the increased field harmonics.

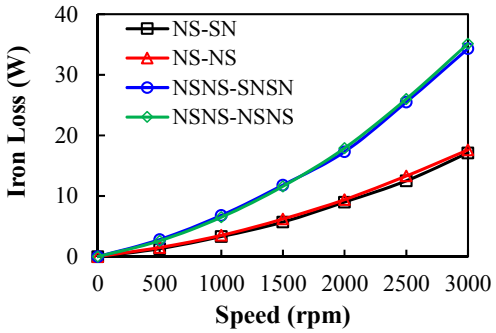

Fig. 22. Full-load iron loss variation against speed. (p_{cu}=20W)

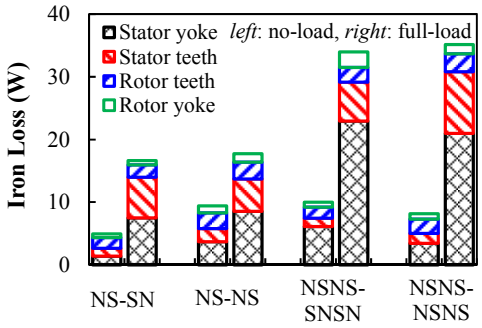

Fig. 23. Iron loss distribution. (n=3000rpm, p_{cu}=20W)

Fig. 24 shows the full-load PM loss variation against speed. As can be seen, the NSNS-NSNS has the largest PM loss while the NS-NS has the lowest one. Considering the fact that all rotating harmonics in air-gap produce eddy current loss since the magnets are static, the major air-gap field harmonics (with magnitude exceeding 0.1T) of the NS-SN and NS-NS are listed in TABLE IV, and the rotational speed and corresponding frequency of each harmonic are calculated based on (1) and (2). As can be seen, for the NS-SN, there exist three rotating harmonics with different rotational speeds but the same frequency. In contrast, only two rotating harmonics exist in the NS-NS, making the PM loss smaller than the NS-SN. Similarly, TABLE V lists the major full-load field harmonics (with magnitude exceeding 0.1T) of the NSNS-SNSN and NSNS-NSNS. It can be found that the rotating harmonics in the NSNS-

NSNS are more abundant than those in the NSNS-SNSN. Therefore, the PM loss of the NSNS-SNSN is smaller than that of NSNS-NSNS.

Fig. 25 shows the variation of rated efficiency against speed. As can be seen, all machines exhibit the highest efficiency around 2500rpm. With rotor speed increasing from 2500rpm, the efficiencies gradually reduce. Within the speed range of 0-3000rpm, the proposed NSNS-NSNS has the highest efficiency thanks to the improved torque density.

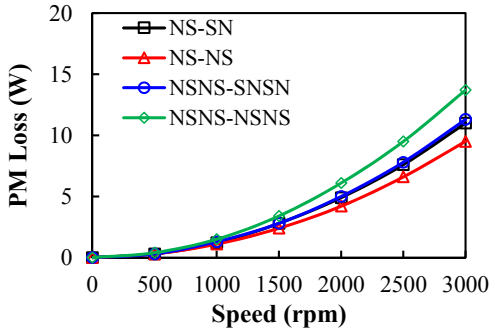

Fig. 24. PM loss variation against speed. (p_{cu}=20W)

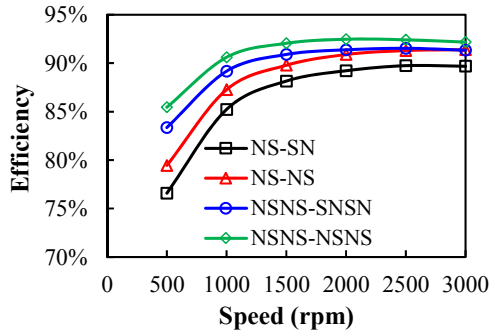

Fig. 25. Efficiency variation against speed.

TABLE IV
FULL-LOAD FIELD HARMONICS OF THE NS-SN AND NS-NS (P_{CU}=20W)

		Static Harmonics			*Rotating Harmonics*		
NS-SN	Order	6th	18th	42nd	4th	8th	20th
	Magnitude	0.66T	0.44T	0.17T	0.13T	0.18T	0.17T
	Speed	0	0	0	-14/4Ω_r	14/8 Ω_r	14/20 Ω_r
	Frequency	0	0	0	f	f	f
NS-NS	Order	12th	36th		2nd	26th	
	Magnitude	0.77T	0.15T		0.21T	0.17T	
	Speed	0	0		14/2Ω_r	14/26 Ω_r	
	Frequency	0	0		f	f	

TABLE V
FULL-LOAD HARMONICS OF NSNS-SNSN AND NSNS-NSNS (P_{CU}=20W)

		Static Harmonics				*Rotating Harmonics*		
NSNS-SNSN	Order	3rd	9th	15th	45th	1st	29th	
	Magnitude	0.28T	0.33T	0.63T	0.14T	0.23T	0.13T	
	Speed	0	0	0	0	-14/1Ω_r	14/29 Ω_r	
	Frequency	0	0	0	0	f	f	
NSNS-NSNS	Order	6th	12th	18th	42nd	2nd	4th	26th
	Magnitude	0.13T	0.7T	0.25T	0.17T	0.23T	0.11T	0.16T
	Speed	0	0	0	0	14/2Ω_r	-14/4 Ω_r	14/26 Ω_r
	Frequency	0	0	0	0	f	f	f

D. Power Factor

Since the PM arrangement influences the average torque and inductance of the FRPM machine, the variation of power factor against torque of four arrangements are compared in Fig. 26. It shows that the NS-SN always has the lowest power factor because of the needed high armature field [15]. Although the NS-NS also needs higher armature field, particularly compared with the NSNS-NSNS, its power factor is the highest, thanks to the smaller inductance (see Fig. 21). It should be noted that because of the low flux linkage per pole [34], the power factor of FRPM machines is relatively low in comparison with conventional rotor-PM machines, especially for the high-torque region. Therefore, additional techniques should be further considered and adopted in FRPM machines when high power factor is required.

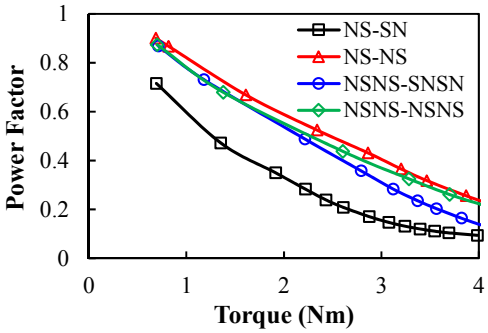

Fig. 26. Power factor variation against torque.

V. EXPERIMENTAL VALIDATION

To verify the previous analyses, four 14-pole-rotor FRPM machines having different PM arrangements are manufactured, as shown in Fig. 27, together with their parameters listed in TABLE I. For simplicity, all the prototypes have the same stator inner diameter and share the same rotor. In addition, the NS-SN and NS-NS share the same stator lamination; the NSNS-SNSN and NSNS-NSNS share the same stator lamination.

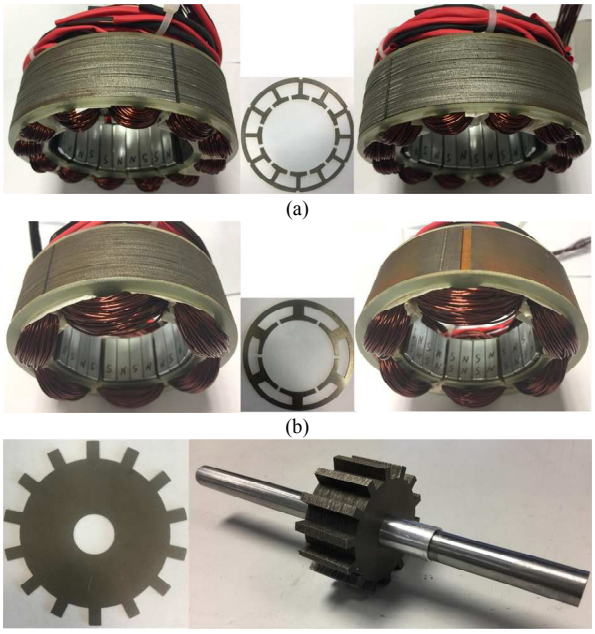

(a) (b) (c)

Fig. 27. Prototype machines. (a) Left: 12-slot NS-SN stator. Right: 12-slot NS-NS stator. (b) Left: 6-slot NSNS-SNSN stator. Right: 6-slot NSNS-NSNS stator. (c) Shared 14-pole rotor.

Fig. 28 shows the measured and FE-predicted back-EMFs of the four machines at n=400rpm. It should be noted that to guarantee the same slot filling factor, the number of turns per coil N_c is 74 for the NS-SN and NS-NS, and it is 115 for the NSNS-SNSN and NSNS-NSNS. As can be seen, the measured back-EMFs match well with the FEA results regardless of PM arrangement, and minor errors can be attributed to the manufacturing tolerance. Test results show that the NSNS-NSNS machine has the highest fundamental back-EMF, which is 72% higher than the NS-SN, 41% higher than the NS-NS, and 10% than the NSNS-SNSN.

By using the simple cogging torque measurement method introduced in [35], Fig. 29 shows the measured and FE-predicted cogging torque waveforms of the four machines. As can be seen, both the measured and FE-predicted cogging torques of the NSNS-SNSN and NSNS-NSNS are larger than the NS-NS and NS-SN.

The variation of static torque against rotor position is measured by supplying three-phase windings with fixed dc current (I_a=-2I_b=-2I_c=I_{dc}=I_{rated}, and the rated current I_{rated} is corresponded to p_{cu}=20W). Fig. 30 shows the measured and FE-predicted static torques against rotor position of four machines. Again, good agreement between the results can be observed. The maximum measured torque of the NSNS-NSNS is 2.3Nm, which is 96% higher than the NS-SN, 64% higher than the NS-NS, and 13% higher than the NSNS-SNSN. The torque variations against current are compared in Fig. 31 as well. As can be seen, the measured torque results match well with the FE-predicted values. Therefore, the improved torque density of the proposed NSNS-NSNS FRPM machine is verified.

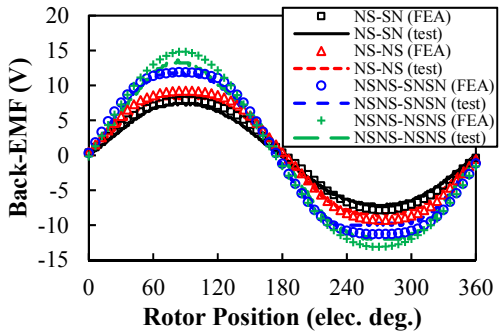

Fig. 28. Measured and FE-predicted back-EMFs. (n=400rpm)

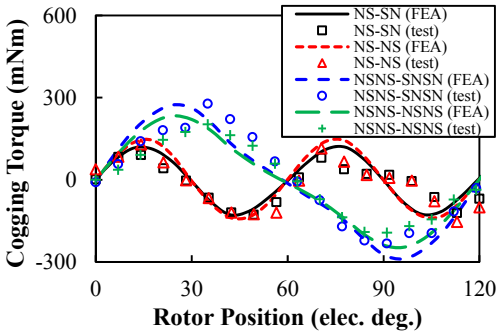

Fig. 29. Measured and FE-predicted cogging torques.

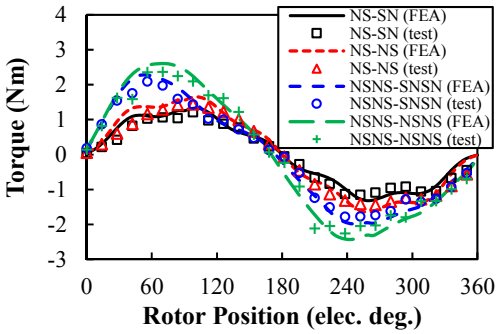

Fig. 30. Measured and FE-predicted static torques. (I_a=-2I_b=-2I_c=I_{rated})

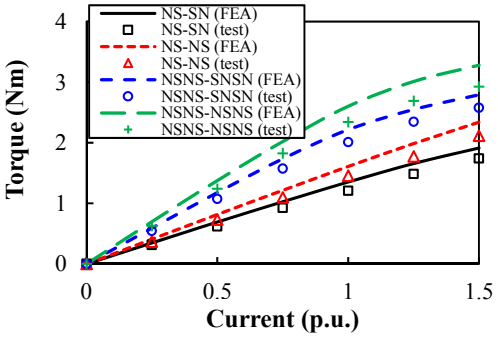

Fig. 31. Torque variations against current.

VI. Conclusion

In this paper, different PM arrangements of FRPM machine are analyzed and compared. Some findings can be summarized as follows: (1) the torque of an FRPM machine is produced by several dominant harmonics, and its performance is greatly influenced by the PM arrangement; (2) in terms of torque density, the optimal rotor pole number is around 14 for the FRPM machines with 12 pairs of PMs, and each PM arrangement is preferable in a specific range of rotor pole number; (3) the torque of machines with four PM pieces on each stator tooth are higher than that of machines with two PM pieces; (4) the FRPM machine of NSNS-NSNS arrangement offers the highest torque density and the highest efficiency when the rotor speed is relatively low. These findings can be useful guidance in designing and analyzing the FRPM machines aiming at good torque performance.

References

[1] M. Cheng, W. Hua, J. Zhang, and W. Zhao, "Overview of stator-permanent magnet brushless machines," *IEEE Trans. Ind. Electron.*, vol. 58, no. 11, pp. 5087–5101, Nov. 2011.

[2] Z. Q. Zhu and J. T. Chen, "Advanced flux-switching permanent magnet brushless machines," *IEEE Trans. Magn.*, vol. 46, no. 6, pp. 1447–1453, Jun. 2010.

[3] Z. Q. Zhu and D. Evans, "Overview of recent advances in innovative electrical machines-with particular reference to magnetically geared switched flux machines," in *Int. Conf. Electra. Mach. Syst. (ICEMS 2014)*, Oct. 2014.

[4] Y. Liao, F. Liang, and A. Lipo, "A novel permanent magnet motor with doubly salient structure," *IEEE Trans. Ind. Appl.*, vol. 31, no. 5, pp. 1069–1078, Sep.-Oct. 1995.

[5] E. Hoang, A. H. Ben-Ahmed, and J. Lucidarme, "Switching flux permanent magnet polyphased synchronous machines," in *Proc. 7th Eur. Conf. Power Electronics and Applications*, vol. 3, 1997, pp. 903–908.

[6] R. Deodhar, S. Andersson, I. Boldea, and T. J. E. Miller, "The flux reversal machine: A new brushless doubly-salient permanent magnet machine," *IEEE Trans. Ind. Appl.*, vol. 33, no. 4, pp. 925–934, Jul. 1997.

[7] I. Boldea, J. Zhang, and S. A. Nasar, "Theoretical characterization of flux reversal machine in low speed servo drives-the pole-PM configuration," *IEEE Trans. Ind. Appl.*, vol. 38, no. 6, pp. 1549–1557, Dec. 2002.

[8] T. H. Kim and J. Lee, "A study of the design for the flux reversal machine," *IEEE Trans. Magn.*, vol. 40, no. 4, pp. 2053–2055, July 2004.

[9] C. Wang, S. A. Nasar, and I. Boldea, "Three-phase flux reversal machine (FRM)," *Proc. IEE. Elec. Power Appl.*, vol. 146, no. 2, pp. 139–146, Mar. 1999.

[10] Y. Gao, R. Qu, D. Li, J. Li, and L. Wu, "Design of three-phase flux-reversal machines with fractional-slot windings," *IEEE Trans. Ind. Appl.*, vol. 52, no. 4, pp. 2856–2864, Feb. 2016.

[11] D. More and B. Fernandes, "Power density improvement of three phase flux reversal machine with distributed winding," *IET Elec. Power Appl.*, vol. 4, no. 2, pp. 109–120, Feb. 2010.

[12] Y. Gao, R. Qu, D. Li, and J. Li, "Design procedure of flux reversal permanent magnet machines," *IEEE Trans. Ind. Appl.*, vol. 53, no. 5, pp. 4232–4241, Apr. 2017.

[13] W. Hua, X. Zhu, and Z. Wu, "Influence of coil pitch and stator-slot/rotor-pole combination on back-EMF harmonics in flux-reversal permanent magnet machines," *IEEE Trans. Energy Convers.*, in press.

[14] T. H. Kim, "A study on the design of an inset-permanent-magnet-type flux-reversal machine," *IEEE Trans. Magn.*, vol. 45, no. 6, pp. 2859–2862, May 2009.

[15] Y. Gao, R. Qu, D. Li, J. Li, and G. Zhou, "Consequent-pole flux-reversal permanent-magnet machine for electric vehicle propulsion," *IEEE Trans. Appl. Supercond.*, vol. 26, no. 4, Jun. 2016.

[16] D. S. More and B. G. Fernandes, "Analysis of flux-reversal machine based on fictitious electrical gear," *IEEE Trans. Energy Convers.*, vol. 25, no. 4, pp. 940–947, Dec. 2010.

[17] R. Qu, D. Li, and J. Wang, "Relationship between magnetic gears and Vernier machines," *Elec. Mach. Syst. (ICEMS 2011), IEEE Int. Conf. on*, Aug. 2011.

[18] D. Li, R. Qu, and J. Li, "Topologies and analysis of flux-modulation machines," *in Proc. IEEE Energy Convers. Congr. Expo.*, 2015, pp. 2153–2160.

[19] W. N. Fu and Y. Liu: 'A unified theory of flux-modulated electric machines', *Proc. Int. Symp. Elect. Eng.*, Dec. 2016, pp. 1–13.

[20] M. Cheng, P. Han, and W. Hua, "A general airgap field modulation theory for electrical machines," *IEEE Trans. Ind. Electron.*, vol. 64, no.8, pp. 6063-6074, 2017.

[21] Y. Gao, R. Qu, D. Li, and J. Li, "Torque performance analysis of three-phase flux reversal machines," *IEEE Trans. Ind. Appl.*, vol. 53, no. 3, pp. 2110–2119, Mar. 2017.

[22] Z. Q. Zhu, "Overview of novel magnetically geared machines with partitioned stators," *IET Electr. Power Appl.*., vol. 12, no. 5, pp. 595–604, Apr. 2018.

[23] H. Li and Z. Q. Zhu, "Influence of magnet arrangement on performance of flux reversal permanent magnet machine," in *Int. Conf. Electr. Mach. Drives (IEMDC 2017)*, May 2017.

[24] D. Li, Y. Gao, R. Qu, J. Li, Y. Huo, and H. Ding, "Design and analysis of a flux reversal machine with evenly distributed permanent magnets," *IEEE Trans. Ind. Appl.*, vol. 54, no. 1, pp. 172–183, Jan. 2018.

[25] G. Pellegrino and C. Gerada, "Modeling of flux reversal machines for direct drive applications," in *Proc. Euro. Conf.Power Electron. Appl.* (*EPE 2011*), Sep. 2011.

[26] K. Atallah and D. Howe, "A novel high-performance magnetic gear," *IEEE Trans. Magn.*, vol.37, no.4, pp.2844-2846, Jul. 2001.

[27] J. X. Shen, H. Y. Li, H. Hao, and M. J. Jin, "A coaxial magnetic gear with consequent-pole rotors," *IEEE Trans. Energy Conv.*, vol. 32, no. 1, pp. 267–275, Mar. 2017.

[28] Z. Z. Wu and Z. Q. Zhu, "Analysis of air-gap field modulation and magnetic gearing effects in switched flux permanent magnet machines," *IEEE Trans. Magn.*, vol. 51, no. 5, May 2015, Art. ID 8105012.

[29] Y. Q. Tang and Y. P. Liang, *Analysis and Calculation of Electromagnetic Field in Electrical Machines*. Beijing, China: CMP, 2010.

[30] J. T. Chen and Z. Q. Zhu, "Winding configurations and optimal stator and rotor pole combination of flux-switching PM brushless AC machines," *IEEE Trans. Energy Convers.*, vol. 25, no. 2, pp. 293–302, Jun. 2010.

[31] S. Chen, *Electrical Machine Design*. Beijing, China: MI Press, 1990.

[32] A. M. El-Refaie, "Fractional-slot concentrated-windings synchronous permanent magnet machines: Opportunities and challenges," *IEEE Trans. Ind. Electron.*, vol. 57, no. 1, pp. 107–121, Jan. 2010.

[33] T. H. Kim, S. H. Won, K. Bong, and J. Lee, "Reduction of cogging torque in flux-reversal machine by rotor teeth pairing," *IEEE Trans. Magn.*, vol. 41, no. 10, pp. 3964–3966, Oct. 2005.

[34] D. Li, R. Qu, and T. A. Lipo, "High-power-factor vernier permanent-magnet machines," *IEEE Trans. Ind. Appl.*, vol. 50, no. 6, pp. 3664–3674, 2014.

[35] Z. Q. Zhu, "A simple method for measuring cogging torque in permanent magnet machines," in *Proc. IEEE Power Energy Soc. Gen. Meet.*, 2009, pp. 1–4.